NARROW BAND OPTIMIZATION OF A COMPTON GAMMA-RAY SOURCE PRODUCED FROM AN X-BAND LINAC*

F. Albert †, D.J. Gibson ‡, S.G. Anderson, R.A. Marsh, S.S, Wu, C.P.J. Barty and F.V. Hartemann,
Lawrence Livermore National Laboratory, Livermore, CA, 94550, USA

Abstract

Nuclear photonics is an emerging field of research that will require high precision gamma-ray (MeV) sources. In particular, nuclear resonance fluorescence applications [1-10] necessitate a low (< 1%) relative gamma-ray spectral width. Within this context, Compton scattering, where laser photons are scattered off relativistic electron beams to produce tunable, collimated gamma rays, will produce the desired gamma-ray output. This paper presents the spectral narrowband optimization of such a light source currently being built at LLNL. In this case, PARMELA and ELEGANT simulations of the high-gradient X-band linac provide the properties of the high brightness electron bunch. The electron beam simulations are then implemented into our newly developed weakly nonlinear Compton scattering code to produce theoretical gamma-ray spectra. The influence that the electron beam, laser beam and interaction geometry parameters have on the produced gamma-ray spectra will be shown with our simulations.

ELECTRON BEAM SIMULATIONS

The electron linac, shown in Figure 2, will comprise an X-band photogun followed by six travelling wave X-band sections. The photoinjector is based on an earlier high-gradient (200 MV/m) 5.5 cell X-band photogun design done by SLAC [10]; it has been implemented to satisfy a high-brightness, narrow bandwidth operation [11]. PARMELA simulations have shown that a longer first half-cell resulted in a lower final emittance for our setup. Hence, the rf gun features are: a longer first half cell (0.59 instead of 0.5), improved mode separation, a dual feed racetrack coupler, optimized coupling, and elliptical cross-section irises. A nominal electron beam normalized emittance of 0.35 mm.mrad (including thermal emittance) is expected at 250 MeV for a beam charge of 250 pC at the interaction point (see Figure 2). Full emittance compensation is implemented, with an optimum distance from the photocathode to the first accelerating section of 0.8 m. This photoinjector is then followed by 6 X-band traveling-wave sections operating at 70 MeV/m. These are the T53VG3 sections, designed and built at SLAC. They are made of 53 cells and operate with a group velocity corresponding to 3% of c, the speed of light. The chicane shown on Figure 2 is implemented only for noise reduction purposes (a block can be placed in the chicane to shield the interaction point from the on-axis Bremsstrahlung arising from the linac).

We also used PARMELA to generate an electron beam phase space distribution at the interaction point. An example is shown in Figure 1. The code uses macroparticles to represent the electron bunch and time steps to push particles. In our simulations, two-dimensional maps of the radio-frequency fields of the accelerator cavities were modeled with the SUPERFISH code and imported into the particle tracker. The space-charge forces are computed using a quasistatic approximation by transforming into a comoving reference frame and computing and applying the Coulomb field on a mesh. For these simulations, 10,000 macroparticles were used. This number was chosen to provide the required resolution for the Compton scattering calculation and to ensure accurate modeling of the electron beam propagation through the accelerator, while maintaining reasonable computation times.

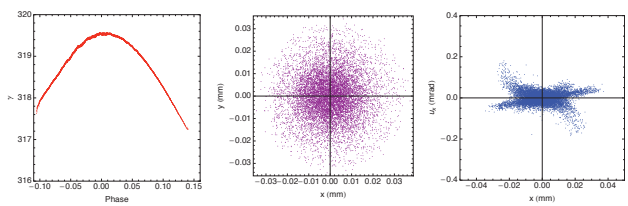

Figure 1: Electron beam parameters simulated with PARMELA.

GAMMA-RAY SIMULATIONS

To predict the gamma-ray source performance from the expected electron beam properties provided by the x-band linac, we have recently developed a full 3D Compton scattering code [12], which calculates gamma-ray spectra on axis for the particular case of a 180 degrees collision between the laser and electron beams. It is valid as long as the product $a_0^2 \Delta\phi << 1$, where a_0 is the normalized vector potential of the laser and $\Delta\phi$ its normalized pulse duration. This code, discussed in details in a recent publication [12], uses the covariant radiation formula which calculates the number of photons radiated per unit frequency dq and solid angle $d\Omega$:

* This work performed under the auspices of the U.S. Department of Energy by Lawrence Livermore National Laboratory under Contract DE-AC52-07NA27344 and supported by the Laboratory Directed Research and Development program under tracking code 12-ERD-057.

† albert6@llnl.gov
‡ presenter

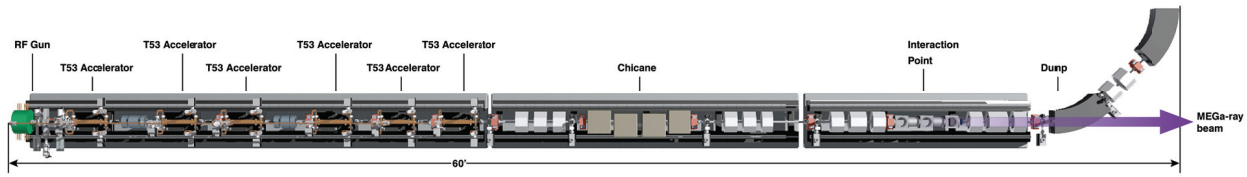

Figure 2: 250 MeV electron linac.

$$\frac{d^2N}{dqd\Omega} = \frac{\alpha}{4\pi^2} q \left| \int_{-\infty}^{+\infty} \pi_\mu u^\mu e^{-iq_\nu x^\nu} d\tau \right|^2 . \quad (1)$$

Here, $\alpha = 1/137$ is the fine structure constant, q is the scattered photon frequency, π_μ is the 4-polarization of the incident laser beam, u_μ is the 4-velocity of the incident electron beam and x_μ its 4-trajectory, obtained by integrating the 4-velocity. In order to evaluate this expression, one needs to know the electron trajectories (velocity and position) at all times as they interact with the laser electrical field. The electron trajectories can be obtained with two different methods: either numerically by solving the differential equation of motion with a 4th order Runge-Kutta algorithm or analytically by using paraxial, ballistic and slowly varying envelope approximations. Both methods have shown excellent agreement for weakly nonlinear ps laser pulses interacting with 100-300 MeV electron beams. For each particle provided by the PARMELA simulations, the photon spectra are added incoherently to yield the on-axis spectrum, using the parameters of Table 1.

Table 1: Laser and Electron Beam Parameters

Parameter	Laser	Electron Beam
Wavelength/Energy	1064 mm	163 MeV
Energy/Charge	0.15 J	250 pC
Focal Spot	10 μm (FWHM)	7.2 μm (rms)
Norm. emittance	N.A.	0.35 mm.mrad

NARROW BAND OPTIMIZATION

Because of the typically large relativistic factor $\gamma \sim 500$ of the electron beam, an electron beam with even a small angular spread $\Delta\epsilon$ (large emittance or tight electron beam focus) will considerably broaden the gamma-ray spectrum. Figure 3 compares two gamma-ray spectra obtained from an electron beam with a normalized emittance of $\epsilon_n = 0.35$ mm.mrad and $\epsilon_n = 1.6$ mm.mrad, respectively. All other laser and electron beam parameters are identical to those given in Table 1. The bandwidth dramatically increases from $\sim 0.7\%$ to $\sim 5\%$. The other important electron beam parameter resulting in gamma-ray spectral broadening is the electron beam energy spread. Figure 4 also shows two gamma-ray spectra obtained from an electron beam with an energy spread $\Delta\gamma/\gamma = 0.16\%$ and $\Delta\gamma/\gamma = 0.25\%$, respectively. We do not expect the electron beam energy spread to be significantly higher for the X-band linac currently under construction. As it can be seen in Figure 4, the energy spread will be less detrimental to the gamma-ray bandwidth in our case.

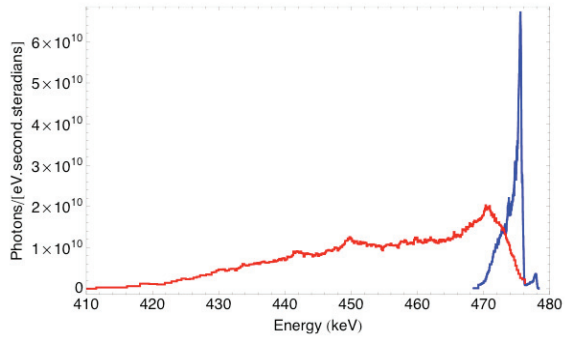

Figure 3: Comparison of gamma-ray spectra obtained for electron beams with two different normalized emittances, 0.35 mm.mrad (blue) and 1.6 mm.mrad (red). Other parameters identical to Table 1.

The final adjustment to the gamma-ray spectral bandwidth can be made with the focusing geometry of the laser and electron beams. For a given normalized emittance, a tighter electron beam focus means a larger electron beam angular spread and thus a wider gamma-ray bandwidth. Similarly, for a given laser energy, a tighter laser focus results in increased nonlinear effects and thus also a wider gamma-ray bandwidth. The resulting spectra from three different focusing geometries are shown in Figure 5, all other parameters being identical. For each case the laser focus is matched to the electron beam focus to maximize the total x-ray flux. The corresponding electron beam focal spots (*rms*) and laser focal spots (FWHM) are 7.2 μm, 14.5 μm, 28.9 μm and 10 μm, 15 μm, 18.6 μm respectively. The corresponding laser normalized potentials are 0.06, 0.04 and 0.03. For the tighter focii, the increase in gamma-ray bandwith is due to both nonlinear effects [13] and electron angular spread. Although the total x-ray

ISBN 978-3-95450-115-1

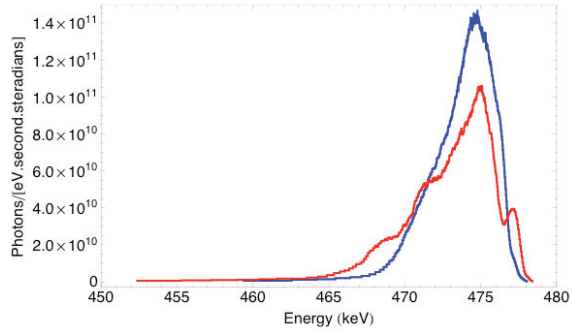

Figure 4: Comparison of gamma-ray spectra obtained for electron beams with two different electron beam energy spreads, 0.16% (blue) and 0.25% (red). Other parameters identical to Table 1.

flux is reduced when opening the electron beam focus, this simulation shows that it is preferable to weakly focus the electron and laser beams in order to maximize the number of photons per unit frequency near the axis. Indeed, the weaker focus case of Figure 5 exhibits a relative bandwidth of $\sim 0.3\%$.

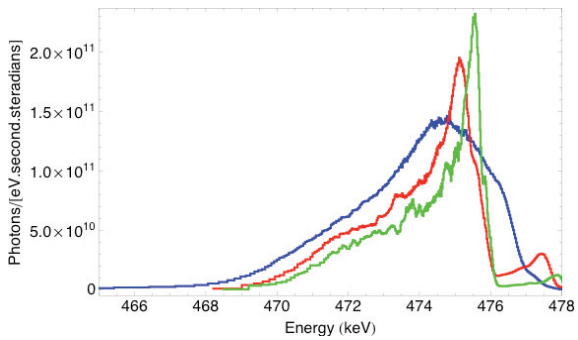

Figure 5: Comparison of gamma-ray spectra obtained for different electron beam focal spots (matched to the laser focal spot): 7.2 μm, 14.5 μm and 28.9 μm. Other parameters identical to Table 1.

CONCLUSION

We presented the theoretical design and narrow-band operation of a Compton scattering gamma-ray source. Within the specific context of nuclear resonance fluorescence (NRF) applications, it is necessary to have a narrow-band gamma-ray operation to enable efficient detection of the narrow ($\Delta E/E \sim 10^{-6}$) NRF lines. NRF is a very powerful isotope-specific process that has potential high impact applications in homeland security, nuclear waste assay and management, stockpile surveillance or medicine. In order for this process to be fully efficient, it is necessary to operate in a spectrally narrow regime. In order to assess spectral broadening mechanisms in Compton scattering, detailed theory and modeling are necessary.

REFERENCES

[1] U. Kneissl, H.M. Pitz and A. Zilges, Prog. Part. Nucl. Phys., 37, pp 349-433 (1996).

[2] W. Bertozzi, *et al.*, Phys. Rev. C, 78, 041601(R) (2008).

[3] C.A. Hagmann, *et al.*, J. Appl. Phys. 106, 084901 (2009).

[4] N. Kikuzawa, R. Hajima, N. Nishimori, E. Minehara, T. Hayakawa, T. Shizuma, H. Toyokawa, and H. Ohgaki, Appl. Phys. Express 2, 036502 (2009).

[5] F. Albert, S.G. Anderson, G.A. Anderson, S.M. Betts, D.G. Gibson, C.A. Hagmann, J. Hall, M.S. Johnson, M.J. Messerly, V.A. Semenov, M.Y. Shverdin, A.M. Tremaine, F.V. Hartemann, C.W. Siders, D.P. McNabb and C.P.J. Barty, Opt. Lett, 35, 3 354 (2010).

[6] D. J. Gibson, F. Albert, S. G. Anderson, S. M. Betts, M. J. Messerly, H. H. Phan, V. A. Semenov, M. Y. Shverdin, A. M. Tremaine, F. V. Hartemann, C. W. Siders, D. P. McNabb, and C. P. J. Barty, Phys. Rev. STAB 13, 070703 (2010).

[7] F. Albert, S. G. Anderson, D. J. Gibson, C. A. Hagmann, M. S. Johnson, M. Messerly, V. Semenov, M. Y. Shverdin, B. Rusnak, A. M. Tremaine, F. V. Hartemann, C. W. Siders, D. P. McNabb, and C. P. J. Barty, Phys. Rev. STAB 13, 070704 (2010).

[8] W. Bertozzi, S. E. Kobly, R. J. Ledoux, and W. Park, Nucl. Instrum. Methods Phys. Res. B 261, 331 (2007).

[9] J. Pruet, D.P. McNabb, C.A. Hagmann, F.V. Hartemann and C.P.J. Barty, J. Appl. Phys. 99, 123102 (2006).

[10] C. P. J. Barty and F. V. Hartemann, "T-REX: Thomson-Radiated Extreme X-rays, Moving X-Ray Science into the 'Nuclear' Applications Space with Thompson Scattered Photons," UCRL-TR-206825, Lawrence Livermore National Laboratory (September 27, 2004).

[11] A. Vlieks, et al., in High Energy Density and High Power RF: 5th Workshop, AIP CP625, p. 107 (2002).

[12] R. A. Marsh et al, submitted to Phys. Rev. STAB (2012).

[13] F. Albert, S.G. Anderson, D.J. Gibson, R.A. Marsh, C.W. Siders, C.P.J. Barty and F.V. Hartemann, Phys. Plasmas, 18, 013108 (2011).

[14] F.V. Hartemann, F. Albert, C.W. Siders and C.P.J. Barty, Phys. Rev. Lett., 105, 130801 (2010).